Engineering Applications of Artificial Intelligence 153 (2025) 110961

Contents lists available at ScienceDirect

Engineering Applications of Artificial Intelligence

journal homepage: www.elsevier.com/locate/engappai

Explainable deep learning model with the internet of medical devices for early lung abnormality detection

Xin Hou [a,*], Nisreen Innab [b], Saad Alahmari [c], Meshal Shutaywi [d], Sara A. Althubiti [e], Ali Ahmadian [f,g]

[a] Department of Oncology, The First Affiliated Hospital of Henan University, Kaifeng, Henan Province 475000, PR China
[b] Department of Computer Science and Information Systems, College of Applied Sciences, AlMaarefa University, Diriyah, 13713, Riyadh, Saudi Arabia
[c] Department of Computer Science, Applied College, Northern Border University, Arar, Saudi Arabia
[d] Department of Mathematics, College of Science & Arts, King Abdul Aziz University, Rabigh, Saudi Arabia
[e] Department of Computer Science, College of Computer and Information Sciences, Majmaah University, Al-Majmaah, 11952, Saudi Arabia
[f] Faculty of Engineering and Natural Sciences, Istanbul Okan University, Istanbul, Turkey
[g] Jadara University Research Center, Jadara University, Jordan

ARTICLE INFO

Keywords:
Convolutional neural networks
Enhanced particle swarm optimization
Deep learning
Internet of medical things
Multi-layer convolutional neural network
Artificial intelligence
Lung cancer detection

ABSTRACT

The decision-making process in healthcare monitoring systems has extensively used deep learning and the Internet of Things (IoT). Among the new uses in today's procedures is disease prediction. A difficult challenge in computer-aided diagnosis (CAD) is lung cancer prediction, which is addressed in this paper's solution using deep learning and IoT. IoT medical devices send disease-related data to the server, as lung cancer is a hazardous medical condition that must be detected faster. Following processing, a multi-layer Convolutional Neural Network (ML-CNN) model is used to classify the medical data into benign and malignant groups. Enhanced Particle swarm optimization (EPSO) is also used to enhance learning capacity (accuracy and loss). Medical data from the Internet of Medical Things (IoMT), including sensor data and Computed Tomography (CT) scan results, is used in this stage. The information from sensors and IoMT devices' picture data is collected for this purpose, and classification operations are then performed. The suggested method's accuracy, precision, sensitivity, specificity, F-score, and computation time are compared to well-known current approaches such as the Support Vector Machine (SVM), Probabilistic Neural Network (PNN), and Convolutional Neural Network (CNN). Linear Imaging and Self-Scanning Sensor (LISS) and Lung Image Database Consortium (LIDC) datasets were the two lung datasets used for this performance evaluation. Trial results indicate that the recommended strategy may aid in the timely and accurate identification of lung cancer in radiologists compared to other techniques. The efficacy of the suggested ML-CNN was examined through Python analysis. The results showed that the accuracy was superior to the number of instances, the precision was superior to the number of cases, and the sensitivity was superior to several instances, the F-score was superior to the number of cases, the error rate was inferior to the number of cases, and the computation time was inferior to the total number of instances computed for the proposed work, even when accounting for prior knowledge. Previous efforts are outperformed by this method, as shown by the suggested ML-CNN architecture.

1. Introduction

Early identification greatly improves lung cancer survival rates and treatment results. However, existing diagnostic techniques often fail to detect the disease in its early stages, causing therapy to be delayed. To address these limitations regarding existing studies, therapists are encouraged to shift towards advanced AI-based technologies in healthcare.

The growth of sensor systems and Internet of Things (IoT)-based medical services have generated a plethora of new research subjects. The

This article is part of a special issue entitled: XAI: methods and applications - MGE: Ahmad Taher Azar published in Engineering Applications of Artificial Intelligence.

* Corresponding author.
E-mail address: houxin8201@163.com (X. Hou).

https://doi.org/10.1016/j.engappai.2025.110961
Received 19 August 2024; Received in revised form 24 March 2025; Accepted 21 April 2025
Available online 29 April 2025

literature now in publication covers IoT, cloud services, and intelligent systems (SIs), transforming conventional health services into intelligent healthcare. Health professionals may improve their practice by utilising vital technology like artificial intelligence (AI) and SIs (Bharathy and Pavithra, 2022). A multitude of choices are made possible by the convergence of IoT and AI in the healthcare sector. The current work suggests a novel AI- and IoT-based sickness diagnosis paradigm for intelligent health systems. The medical centre has to transition to a user system as soon as feasible because of the high cost of health insurance and the incidence of several ailments (Abd et al., 2022). Researchers have shown that early cancer detection significantly increases survival rates. However, it might be challenging to identify these diseases early. Half of the cancer patients are estimated to be in the middle or late stages of the illness based on accurate categorisation (Feng et al., 2024). The basic approach outlined below is often used for medical image processing-based illness diagnosis.

- Picture Preprocessing: This stage involves making rotation, scale, and translation corrections to enhance the quality of the picture by eliminating unwanted distortions. Some crucial preprocessing tasks include normalization, contrast enhancement, denoising, and more (Patil et al., 2023).
- Feature extraction is the procedure that this phase uses to turn the input data that has been provided into a collection of features. Feature extraction is carried out on borrowed values known as features in medical image processing, and it begins with the first set of trustworthy data (Hu et al., 2025). This significantly improves the prediction quality of the categorisation approach. Most medical image classifiers rely on Computer-aided diagnostic (CAD) feature extraction results.
- Feature selection: This stage shortens the feature space taken from the whole picture, improving detection efficiency and reducing execution and reaction times. A smaller feature space is achieved by eliminating duplicate, noisy, and irrelevant characteristics and selecting the feature subset that performs well across all measures. At this point, dimensionality is decreased (Huang et al., 2022).
- Classification: Each sample is classified using the chosen characteristics to indicate the intended class. Nonetheless, a significant problem in medical image analysis jobs is categorisation. Optimal feature sets are employed for automated categorisation; nevertheless, more improvements in this stage are necessary for a more comprehensive clinical study of the human body for disorders (Duan et al., 2023). Computer-aided diagnostic solutions have shown efficacy in identifying issues more quickly and precisely. Regretfully, several errors and ambiguities in this diagnostic method might result in an incorrect diagnosis. Information from IoT sensors is, therefore, combined with the categorisation model. Currently, lung illness is detected in computerised tomography (CT) pictures using machine learning (ML) models. Fig. 1 displays the pipeline design. The essential contributions of the work are as follows (Rajasekar et al., 2023):
- Better CNN Model: The CNN's calculation is optimized to increase lung cancer diagnostic performance based on various inputs. Based on the retrieved characteristics, the CNN determines the enhanced range of values (Li et al., 2024a).
- Hyperparameter tuning: The CNN's learning parameters must be generated on demand. The particle swarm optimization (PSO) technique is used to modify the hyperparameters, which is also considered an optimization issue (Pandian et al., 2022; Su et al., 2022; Sivakumar et al., 2024).
- Notable improvements in diagnosis complexity in terms of performance: the optimized CNN design has fewer convolutional layers since it considers relevant data from the max-pool, fully connected, and convolutional layers. Because of the central structural perspective of the CNN, the suggested optimized CNN may achieve minimum complexity (Hosseini et al., 2024; Li et al., 2024b).

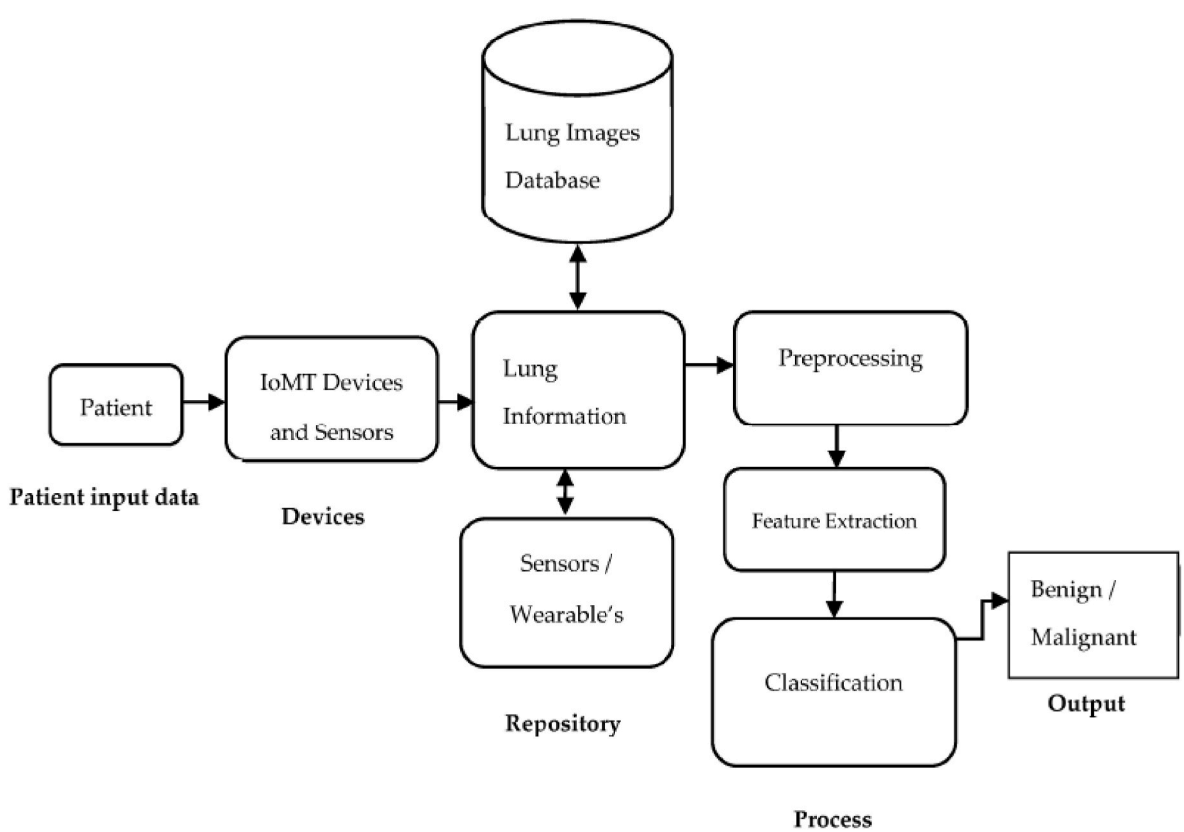

Fig. 1. IoMT-based lung disease diagnostic pipeline.

- IoT sensor and medical image consideration: Lung cancer is diagnosed from pictures using sensor data and medical images (Jiang et al., 2024; Zaidi and Sushma, 2023). Together with the study model architecture, Fig. 1 displays the pipeline for IoMT-based lung disease diagnostics. A clear roadmap for the scientific endeavour has been provided.

1.1. Motivation for lung cancer research

Every day, victims of the illness, who are from all across the nation, lose their identities, their joys, and their precious quality of life. These factors motivated us to investigate the necessity for early illness diagnosis and to identify and evaluate the disease's underlying causes. Examine the fundamental causes of the illness and the need for lung cancer early diagnosis. This inspired us to start looking into lung cancer right away. Below is a summary of other factors.

➢ An earlier diagnosis may increase a patient's chances of survival and standard of living.
➢ Research can help those diagnosed with lung cancer live better and longer lives.
➢ Ultimately, it may also increase the number of people who survive.

When referring to one or more specialised diagnostic procedures, "advanced imaging" refers to the ability to see the inside organs and tissues of the body. CNN automatically determines vital qualities without any human supervision. Utilising a convolution neural network (CNN), a multi-layer perceptron has been developed to automatically learn the distribution law of data from an enormous dataset.

The convolutional neural network (CNN) uses a large amount of data to identify the intricate representation of visual input. The human visual system influences it since people can see colour. Convolutional networks interpret images as volumes, which correspond to three-dimensional objects. The colour spectrum in digital images combines Red, Green, and Blue (RGB) encoding. Before going on to the next layer, each layer generates a dot product of the input pixels. The following levels of activities are included in the CNN in addition to the basic framework.

Particles are the possible solutions in particle swarm optimization (PSO). The optimum choice occurs when particles move across the issue space and are connected to fitness or the ideal state. It tracks all the coordinates of each particle likewise. This fitness value is now referred to as Pbest. A particle is considered the best if it accepts the whole population as its neighbour, in which case its value is the best overall.

The study project's components are as follows: (2) primary knowledge, which helps the reader grasp the main idea; (3) related works, which piece together the main ideas; (4) system model, meant for the essential features; (5) experimental results and discussion, where the results are extensively discussed; and (6) the conclusion, which covers the findings, points of view, and references for a basic understanding of the work.

The contribution of the research lies in.

- This research provides a new range of IoT medical devices capable of diagnosing lung cancer at its inception stage by imaging data constantly collected remotely over the Internet.
- In this work, IoMT devices such as medical sensors and CT scan images were used to gather real-time data for the detection of lung cancer. Integrating deep learning, particularly Multi-layer Convolutional Neural Networks (ML-CNN), with IoMT for the automation and precise classification of lung cancer is a novel development that has not been adequately investigated in the literature.
- It puts forth Enhanced Particle Swarm Optimization (PSO) as one of the improvement measures for amplifying the efficiency of deep learning models in the context of healthcare diagnosis.

The remainder of the paper follows this format: Section 2 covers the basic understanding of lung cancer detection techniques. Section 3 delineates the corresponding research, providing more details on the most advanced techniques now available for lung cancer categorisation.

Section 4 presents a system model for diagnosing lung cancer. Section 5 covers the experimental findings for the suggested and current approaches. Section 6 ends the study by explaining future work.

2. Fundamental understanding

The categorisation techniques used today may be categorized as either supervised or unsupervised. Gaussian kernels are employed in support vector machines (SVM) to perform transformations when no previous input knowledge is available. The listed researches all make use of Random Forest. The best method for identifying the best model is support vector machines (SVM), which are gaining popularity due to their effectiveness and speed of processing. An SVM method designed for lung cancer illness needs a lengthy processing time and does not handle small-scale datasets (Lin et al., 2016).

The advancement in transfer learning and fine-tuning approaches has led to enhanced automated segmentation of image components, such as the area of interest in diagnostic pictures (Hasenleithner and Speicher, 2022). This data-collecting process combines deep learning and artificial intelligence algorithms to create statistics. Experts then analyse the data to assist clients in living better lifestyles and preventing disease. Among the most current advancements in gathering patient data are health records (HRs), Internet of Things (IoT) sensor systems, mobile and personal phones, internet data, and social networks. The PH employs the created data set to improve self-regulation and the self, sickness prediction, self-development, and therapeutic intervention processes via artificial intelligence (AI) techniques (Trivedi et al., 2022). Recent research has examined IoT devices in the healthcare industry. Aids in healthcare diagnostics are commonplace. Early diagnosis is critical for improving the prognosis of lung cancer patients. Deep learning and machine learning are widely used to identify lung illness and perform screening. Examining how deep learning contributes to lung illness identification and diagnosis is the main objective of this work. To identify lung illness utilising radiographic imaging, we used a convolutional neural network (CNN), a form of deep learning model (Wang et al., 2025). To locate and classify the lung spikes and assess their level of hazard, a CT scan of the lungs may be performed. Although an upgraded CNN is less responsive to setup than previous frameworks, it offers substantial accuracy and temporal complexity features. There are tumours on them.

3. Related work

This research included a scan of around 36 papers that used computational approaches (Manickam et al., 2022) to predict different illnesses. The study uses a range of neural network models to detect several diseases and spot any gaps in the current understanding of lung disease in the context of healthcare IoT. The general drawbacks of each approach were determined after a step-by-step analysis. Reviewers also looked at the kind of data benchmark or manually collected to forecast the illness under consideration. Finally, based on many approachable methods, tactics are designed and shown. This will help future studies find cancer patients in their early stages and accurately identify them without any flaws.

In (Li et al., 2018), the authors suggest an effective support vector machine (SVM) for lung classification. They modify the SVM's properties and extract features by using a genetic algorithm and an improved gray wolf optimization method (GWO-GA). Three groups make up the experimental phase: optimum SVM, feature engineering, and parameterisation testing. The approach's efficacy was evaluated using a benchmarking picture dataset of fifty low-dose and archival lung CT scan images. The provided work illustrated the performance of the whole sample picture collection in several ways. In addition, its accuracy rate of 93.54 % is much higher than that of the assessed methodologies.

A unique Internet of Things-based prototype for the feature extraction and categorisation of computed pulmonary tomography is presented in this work. The proposed method uses the Internet of Medical Things, a Software Development Kit (API), in conjunction with the backpropagation algorithm and Parzen's probability density to detect lung pictures. With almost 98 % of lung image classifications correctly, the approach was practical. Next, the model applies the lung segmentation approach, which builds a lung map and employs Masks Regional-CNN network fine-tuning to identify the pulmonary borders on the CT image. The notion was validated, as the proposed method achieved classification parameters like 98.34 % (Li et al., 2023), surpassing earlier research attempts in the field.

Once again, a probabilistic neural network (PNN) was used for diagnosis, and computed tomography (CT) pictures of the lungs were used for assessment. Following the preprocessing of the raw lung pictures, characteristics are retrieved using the Gray-Level Co-Occurrence Matrix (GLCM).

The characteristics are selected using the chaotic crow search algorithm (CCSA), which is given. Accuracy, predictive value, sensitivity, and precision were the computation measures used.

Based on the experiment, feature selection using CCSA successfully approaches 90 % of images with unevenly distributed cells. In certain cancers, abnormal lung development and degeneration lead to the growth and expansion of cancer cells, which ultimately form a tumour. Airborne toxins damage lung tissue whenever they come into touch with it. Computer-aided automated diagnosis is now challenging due to the characteristically vague lung cancer nodule. A selection strategy to extract essential features was used with average accuracy to enhance the classification performance. According to the findings, the PNN with CCSA-based selection features performs better than the PNN without such features (Arumugam et al., 2022).

To improve health by providing medical recommendations and anticipating lung cancer development via continuing analysis, researchers presented a new Internet of Things (IoT)-based prediction model based on fuzzy-cluster-based enhancement and classification. The energy that may be transmitted via extraction is the basis for the fuzzy clustering technique used for effective image segmentation. Furthermore, the transition area features are classified from the lung cancer image features using the Fuzzy C-Means Clustering approach. This technique recovers the transition zone from a lung picture using the Otsu thresholding strategy. Furthermore, the morphology reduction process and right-hand-side photos are used to enhance the accuracy of segmentation (Luan et al., 2023).

The lung image on an edge was subjected to morphology cleaning and image region filling techniques to get the image areas. The authors also provide a new continuous classification method combining a CNN, a traditional Decision Tree (DT) with feature representation, and already-existing Association Rules (ARM). To solve the problem, LungNet, a novel hybrid Deep Neural Network (DNN)-network-based framework constructed utilising CT scans and healthcare IoT data gathered using a wearable camera, is presented. LungNet is a 22-layer CNN model that combines MIoT data with latent features extracted from CT scan images to enhance the system's detection performance. This system can identify lung illness into five categories with high accuracy (96.81 %) and a lower false-positive rate (3.35 %) than similar CNN-based classifications. It is operated from a centralised server and was trained using a balanced dataset of 525,000 pictures. Additionally, it correctly classifies lung tumours in phases 1 and 2 into subclasses 1A, 1B, 2A, and 2B with a probability of 10.5 % detection rate (Yu et al., 2023).

This system's gadgets are all sensitive to volatile organic compounds (VOCs), which have been linked to lung cancer. Before use, the device's data needed to be standardised. Features were then gleaned from the data to enhance classification performance. Principal component analysis was used to remove unnecessary traits. The gathered attributes were classified using the k-nearest Neighbourhood and Support Vector Machine models (Vishwa et al., 2023).

Utilising quantitative research employing lung identification and treatment, automated learning was developed in this study using computed tomography (CT) pictures. The proposed model uses a preprocessing strategy based on Gaussian filtering (GF) on CT samples obtained from a lung dataset. In addition, the normalized cuts (Nuts) approach is used, which has the potential to identify nodules that were present before the picture capture. Furthermore, the orientated FAST and rotated BRIEF (ORB) approach is used as a feature extractor. The sunflower optimization-based wavelet neural network (SFO-WNN) model is the last model for diagnosing lung cancer diagnosis. The diagnostic results of the Machine Learning with Data Science (MLDS)-Lung Cancer Diagnosis and Classification (LCDC) model were assessed by descriptive analysis and evaluated according to several criteria (Xu et al., 2022).

This research suggests using optimum computer-aided diagnostics for lung illness that is automated. The process starts with the input photos being normalized and noise removed. The next step is the division of pulmonary regions using classification and Kapur entropy maximisation algorithms. Nineteen Gray-Level Co-Occurrence matrix (GLCM) features were extracted from the segmented pictures and used in the remaining portion of this investigation. The most critical photos were selected to make the program less complicated. The feature selection method is a novel optimization technique called Enhanced Thermal Exchange Optimizations (ITEO) to boost stability and dependability. ITEO uses an enhanced artificial neural network to categorise photos into benign and malignant conditions (Lin and Tan, 2023).

Despite their widespread usage in the past, positron emission tomography (PET), computed tomography (CT) scans, ultrasound devices, and magnetic resonance imaging (MRI) all have serious drawbacks, including expense and radioactive material exposure. Sensor synchronisation in processing has lately been used in advanced screening because of its affordability, accessibility, and ease of use. Intelligent sensor innovation has been realised, and biotechnologies are becoming standard instruments for cancer scares in the medical field. The findings of research on biosensing's application to lung cancer therapy are presented in this article. According to the study, the electrochemical biosensor is the most popular method for diagnosing lung cancer in its early stages (Lydia and Prakash, 2023).

This article presents a novel deep-learning method for lung cancer diagnosis by combining kernel k-means clustering with a convolutional neural network (CNN).

The suggested approach was evaluated using the Anti-PD-1 Immunotherapy Lung datasets from The Medical Image Archives (data retrieved on October 19, 2022, from https://www.kaggle.com/datasets/nih-chestxrays/and https://comport.com/healthcare-it-solutions/medical-image-archives/). The researchers used 400 MRI pictures from these data, which were meticulously categorized. Among these were 250 images of cancer and 150 photos of ordinary lung scans. The initial phase was the analysis of the data using the framework. The kernel k-means clustering method flattens neurons in the feature space for every picture produced by the CNN's convolution process. This technique yields the prediction classification of each piece of data in the cross-validation, and it is used to find the centre of each cluster once again. K-fold cross-validation was performed using a variety of data points to evaluate the efficacy of the recommended strategy. With nine-fold cross-validation and kernel functions with sigma = 0.05, the suggested method produced the best set of metrics: 98.85 %, 98.32 % sensitivity, 99.40 % accuracy, 99.39 % specificity, and a 98.86 % F1-measure (Thanoon et al., 2023).

An intensive CAD system for cancer diagnosis using breast tomography images was built in this research (CNNs) using enlarged SegNet and convolutional neural network models. An expanded SegNet model was used to separate the lung from chest CT images, and a CNN model with batch normalization was developed to separate the true nodules from all possible nodules. The extended CNN and SegNet classifiers were trained using sample instances from the Lung Nodule Analysis (LUNA) 16 dataset (https://luna1 6. grand-challenge.org/, retrieved on October 19, 2022). The Dice coefficient measured the segmented model's effectiveness, and the nodule classification was evaluated using sensitivity analysis. The accuracy of feature identification achieved using CNN classification was validated by statistical methods (Kapatia et al., 2023).

Additional research produced a mixed network for lung lesion detection and identification that can simultaneously recognise, segment, and classify pulmonary nodules while considering the training dataset's intrinsic labelling errors. It enables the segmentation of nodules that are found as well as the final identification of nodules. The suggested integrated system's nodule detection and classification subnets use a 3-Dimensional (3D) encoder-decoder architecture for enhanced 3D data processing. Additionally, by using features taken from the detection subnetwork with multiresolution nodule-specific data, the classification subnet strengthens the categorisation model. In contrast to the existing backpropagation approach, the suggested technique offers valuable historical information to optimise the more complex 3D classifier correlational design and more accurately detect problematic clusters from several tissues (Yan et al., 2023).

A hierarchy attention-based multiple instance learning (HA-MIL) paradigm was created for patients identifying the illness by integrating two feedforward attentiveness processes: one at the nodule level and the other at the item level. Building on the representations of key components and nodule information, the proposed HA-MIL platform combines lung identification with nodule representation. The general public Lung Image Database Consortium and Set of Images Resource Initiative (LIDC-IDRI) dataset (https://paperswithcode.com/dataset/lidc-idri, accessed on October 19, 2022) showed that the HA-MIL framework outperformed previous methods, such as higher transaction learning in the case of MIL and embedding-space MIL. This proved the effectiveness of hierarchy ensemble learning. The data analysis (Malik et al., 2023) indicates that the HA-MIL model identified significant nodules and attributes using higher attention weights.

Exact symptom characterisation is essential to treatment in Traditional Chinese Medicine (TCM), a promising therapy for lung illness. Concrete proof of TCM treatment cases and the development of intelligent systems allow for the development of smart algorithms for TCM syndrome classification. The goal is to increase the range of benefits TCM offers for lung malignancies. This work aimed to create end-to-end TCM diagnostic systems that may resemble the categorisation of lung diseases. To use the information obtained by lung specialists for real-world TCM treatment cases, the built models used disorganised patient files as inputs. The produced algorithms performed better than unstructured TCM data (Dodia et al., 2022; Civit-Masot et al., 2022). The articles in the linked work can still improve their correctness and performance even if they already have some relevance. Based on the comprehension obtained from examining the studies above, this study has determined that ML-CNN using PSO and hyperparameters offers increased accuracy, performance, and precision.

SVM with wolf optimization and the genetic algorithm has 93.54 % accuracy; R-CNN with backpropagation algorithm and Par zen's probability density has 98.34 % accuracy; Gray-Level Co-Occurrence Matrix and chaotic crow search algorithm with a probabilistic neural network provide 90 % accuracy; CNN with Association Rules and conventional Decision Tree (DT) provides 96.81 % accuracy; Gaussian filtering with the sunflower optimization-based wavelet neural network has less than 90 % accuracy; Enhanced Thermal Exchange Optimization and Kapur entropy maximisation and classification techniques have less than 90 % accuracy; In nine-fold cross-validation, the convolutional neural network yields an accuracy of 98.32 %.

Nonetheless, out of all the analysed approaches, our ML-CNN with PSO and hyperparameters boffers the most fantastic accuracy at 98.85 %.

The clinical gap highlights the existing study based on specific lung cancer detection problems; the proposed model aims to address challenges based on the existing research scopes. In the related works, various computational approaches, such as Support Vector Machines (SVM), CNN, PNN, and IoT-based systems, have been proposed to detect lung cancer at early stages. However, each of these methods has its limitations. To tackle these issues, we develop our suggested model, which is illustrated in detail in the upcoming sections.

4. System model

This section provides the suggested system model architecture. Lung cancer classification is enhanced using IoMT technology, sensors, and devices. This suggested model is shown in Fig. 2. The architecture of a lung cancer detection system combines IoMT sensors and medical imaging. The procedure starts with raw CT scan images, which are initially preprocessed to improve the data quality using denoising and normalization techniques. Essential features of the lung nodules, such as their shape, texture, and intensity, are retrieved using preprocessing. An ML-CNN model is then used to classify these features and effectively classify benign and malignant nodules. Further, the extracted feature vectors are maintained in a database called StoreDB. Then, the data is collected continuously from IoT sensors and devices, which include wearables and other medical monitors. The sensors undergo Z-score normalization preprocessing to ensure the proper analysis. This data is then transformed into feature extraction, which records relevant physiological values. The ML-CNN model is then used to classify the collected features and assess the exact condition. This integrated system uses CNN-based classification to provide a thorough and effective lung cancer detection solution by combining data from IoMT sensors and CT imaging.

4.1. Explainable deep learning and its advantages

Using supervised machine learning techniques, this study (Alsinglawi et al., 2022) suggests a prediction framework to calculating the Length of Stay (LOS) for lung cancer patients in the intensive care unit. A variety of sampling strategies, like SMOTE and ADASYN, are used to solve the dataset's class imbalance, and the Random Forest model performed better than other models with excellent accuracy. The paper (Wani et al., 2024) presents "DeepXplainer," a hybrid deep learning-based method for detecting lung cancer that combines XGBoost and convolutional neural networks (CNN). After CNN's convolutional layers had learned important features, XGBoost was applied to predict class labels. With a 97.43 % accuracy rate, high sensitivity, and F1-scores, SHAP was used to provide both local and global explanations of the predictions. The goal of this research (Rikta et al., 2023) is to improve the interpretability of machine learning models used for lung cancer detection by applying Explainable Machine Learning (XML) approaches. The diagnosis of lung cancer, obtaining excellent performance like 98.76 % accuracy and 98.79 % precision. The study (Kobylińska et al., 2022) investigates how machine learning models used for lung cancer imaging is enhanced by utilising Explainable Artificial Intelligence (XAI) methodologies. It contrasted three popular models like PLCOm2012, LCART, and Bach which highlights the major factors affecting model predictions.

4.2. Preprocessing

In the preprocessing stage, lung images are denoised using the Bayesian threshold-based Taylor series method, to handle the pixel intensity variations. The Bayesian filtering technique continuously estimates the noise level based on the subband features and make it highly effective in removing noise by preserving important features for disease detection. To start, lung images denoising to improve their quality,

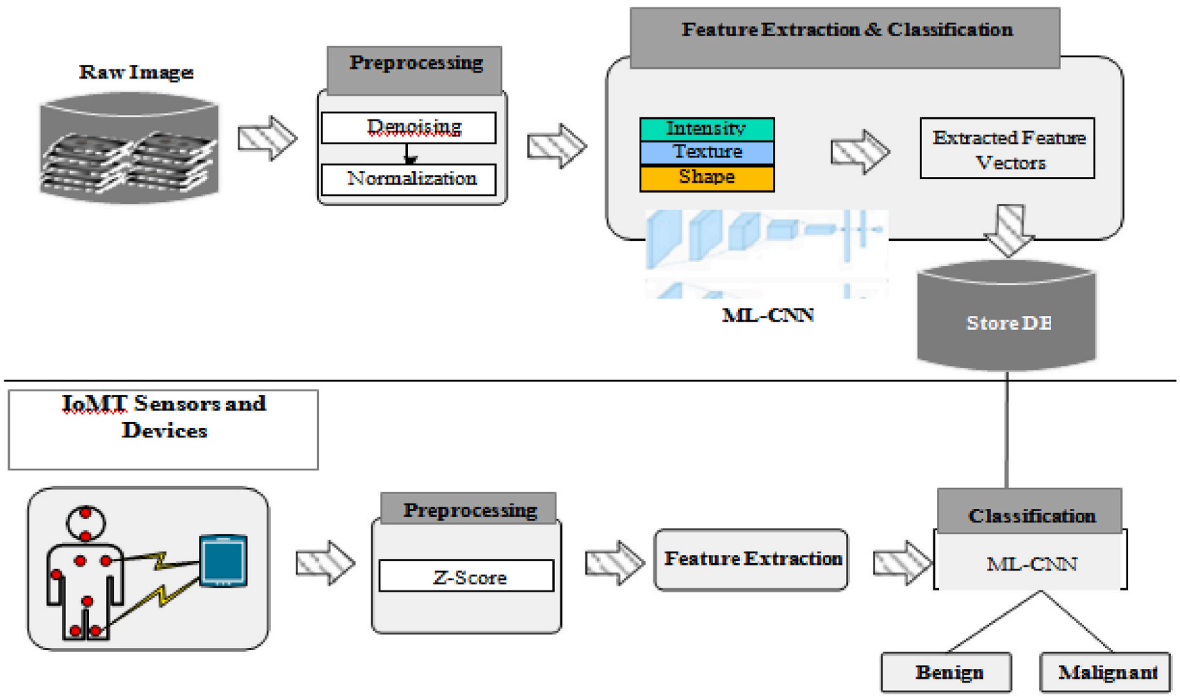

Fig. 2. Architecture of the system.

Taylor series provides high-resolution wavelet subbands, our suggested method is based on it. The infinite sums of terms the Taylor series defines are approximated from derivative functions with varying and pixel-based values. Consequently, the Taylor series for a three-dimensional frame is represented as

$$\mathscr{U}(\mathscr{Y}) = (\mathscr{b}) + (\mathscr{Y}-\mathscr{b})^{\mathscr{U}}\mathscr{C}(\mathscr{b}) + \frac{1}{2!}(\mathscr{Y}-\mathscr{b})^{\mathscr{U}}\{\mathscr{C}^2 f(\mathscr{b})\}(\mathscr{Y}-\mathscr{b}) + \ldots. \tag{1}$$

The design of the system and its roles in fundamental comprehension are elucidated in detail in Fig. 2. The ML-CNN and feature extraction models and other pre-processing principles are explained in Fig. 2.

Because an image's intensities vary throughout, it often has various pixel values. Thus, more consideration for denoising has to be given to the variations in pixel values. Subband noise is calculated from the specified Taylor series and removed if it exceeds the predicted Bayesian threshold. Using the following equation, the threshold for each subband is calculated:

$$\mathscr{U}_{\mathscr{A}} = \frac{\sigma_{\mathscr{T}}^2}{\sigma_{v}} \tag{2}$$

Where $\mathscr{U}_{\mathscr{A}}$ the threshold is determined for each band, and $\sigma_{\mathscr{T}}$ is the noise estimate.

In the case when $\sigma_{v} \neq 0$, it is expressed as

$$\sigma_{v} = \sqrt{\max\left((\sigma_{\mathscr{x}}^2 - \sigma_{\mathscr{x}}^2), 0\right)} \tag{3}$$

$$\sigma_{\mathscr{x}} = \frac{1}{\mathscr{T}}\left(\sum \mathscr{V}\mathscr{A}_j\right) \tag{4}$$

$\mathscr{V}\mathscr{A}_j$ Comprises the subbands $\{\{\mathscr{OOO}, \mathscr{OOG}, \mathscr{OGO}, \mathscr{OGG}, \mathscr{GOO}, \mathscr{GOG}, \mathscr{GGO}, \mathscr{GGG}\}$, which is the total number of subbands; $\sigma_{\mathscr{T}}$ is established by

$$\sigma_{\mathscr{T}} = \left[\frac{median(\mathscr{V}\mathscr{A})}{0.6745}\right] \tag{5}$$

Once the $\mathscr{U}_{\mathscr{A}}$ value has been estimated, the resulting values of the Bayesian threshold are sorted, and an expression is generated as follows using the curve-fitting technique:

$$\gamma = \frac{\mathscr{g}_1\delta^2 + \mathscr{g}_2\delta + \mathscr{g}_3}{\delta + \mathscr{p}} \tag{6}$$

The values of other variables in Equation (6) are $\mathscr{g}_1 = 0.9592$, $\mathscr{g}_2 = 3.648$, $\mathscr{g}_3 = -0.138$, and $\mathscr{p} = 0.1245$. δ denotes the standard noise deviation. After that, the following is the mathematical expression for the block-matching 3D (BM3D) filtering algorithm:

$$\widehat{\mathscr{X}}\mathscr{V}_{\mathscr{V}\mathscr{A}} = \mathscr{U}_{3\mathscr{C}}^{-1}\left(\alpha\left(\mathscr{U}_{3\mathscr{C}}(\mathscr{W}_{\mathscr{V}\mathscr{A}}), \mathscr{U}_{\mathscr{A}}\gamma 2\log\left(\sqrt{\mathscr{T}^2}\right)\right)\right) \tag{7}$$

Equation (7) specifies the threshold operator as α, the subband size as $\mathscr{W}$, the unitary $3\mathscr{C}$ transform as $\mathscr{U}_{3\mathscr{C}}$, and $\widehat{\mathscr{X}}\mathscr{V}_{\mathscr{V}\mathscr{A}}$ as stacked subbands. Based on this final formulation, every subband is rebuilt and given denoised frames for feature extraction.

Equation (12) shows the relative entropy distance measure by $\mathscr{C}_{\mathscr{R}\mathscr{E}}(\mathscr{E}_j, \mathscr{E}_{j+1})$, which also provides the square root of the relative entropy between the frames. The probability distribution function of the frames in a video, or $\mathscr{E}_j$ and $\mathscr{E}_{j+1}$, is represented by the equation $\mathscr{g}_j = \{\mathscr{g}_j(1), \mathscr{g}_j(2) \ldots . \mathscr{g}_j(t)\}$. This function is derived from a normalized intensity histogram of n bins. The bin has a value of n = 256, and k is the total number of frames in each shot. A comparison between the square root of relative entropy and relative entropy-based distance metrics is performed depending on the direction of time. This comparison allows for the identification of frame changes and the removal of excessive frames. Image intensity levels are normalized into equal ranges in this phase to be processed correctly in the subsequent stage. The intensity normalization procedure, ranging from 0 to 1, is carried out in the next phase. Intensity normalization is accomplished using the Z-score normalization function, which performs better than the decimal and min-max normalization methods. The following is the computation of this normalization function:

$$\mathscr{X}_j = \frac{\mathscr{g}_j - \mu}{\sigma} \tag{8}$$

In this case, $\mathscr{g}_j$ denotes the intensity position, μ is the variance, and $\mathscr{X}_j$

stands for the normalized intensity values for the input picture. Intensity normalization was performed using the Z-score normalization function, which was carried out in the reasonable range (0–1) when processing the image for subsequent procedures. For training and testing purposes, this step is required for all images. This reduces the overhead or complexity for comparable medical picture retrieval algorithms with the same attributes, such as size, intensity values, etc.

4.3. Feature extraction

The following features were extracted from the lung images as part of the retrieved characteristics.

- Features that characterize an image's intensity and histogram values (visibility is considered in the grayscale or color intensity histogram) are intensity-based.
- Features based on shape: These provide details on the size and shape of a picture.
- Features that are texture-based: They evaluate the characteristics of smoothness, regularity, and coarseness while describing the fluctuations in image intensity on the surface.

A comparative study was carried out to investigate the efficacy of several strategies, like Gabor filters, Local Binary Patterns (LBP), and Gray-Level Co-Occurrence Matrix (GLCM), to improve the feature extraction process. Gabor filters are well-known for their capacity to discover small lung abnormalities by evaluating spatial frequency to detect texture and edge features. Where the GLCM is used to capture the spatial relationship between pixels, which provides a deeper understanding of lung tissue structure, LBP is a texture descriptor that is useful for identifying patterns in medical images. These techniques are combined together and particularly to improve classification accuracy and to detect finer textures.

During feature extraction, the best collection of features is extracted since a large number of characteristics cannot be processed by the classification technique. Because of this, spatial transformer networks are used to choose the best feature sets from the extracted feature set.

One of the main issues with neural network systems, namely its high training complexity, is the CNN. Loss values determine the need for training, which is often necessary.

The PSO method, which determines the ideal hyperparameter values based on input types and ranges, is presented in this study as a solution to this problem. This kind of integration generates fewer epochs for training and testing with the usage of epochs, which lowers the cost of hardware for CNN training. This, combined with frequent back-propagation approach training, also lowers the local minimum problem. The following is a representation of the CNN's structure.

- The input layer that gathers the inputs, or signals, is called the convolution layer. The purpose of this layer is to quickly handle inputs by normalizing their range into a single value.
- Pooling Layers: This layer aims to reduce input size, automatically affecting improved performance.
- Activation Layer: In non-linear scenarios, this layer maximizes the outputs by using the rectified linear unit (ReLU) activation function.
- Fully Connected Layer: This layer controls the output range using an activation function known as softmax. The weight values between nearby neurons for a particular issue are computed using the suggested CNN.

Fig. 3 depicts the classification and segmentation of images using convolutional neural networks (CNNs), a kind of deep neural network. Supervised and unsupervised machine learning methods may be used to train the CNN. Its integrated convolutional layer lowers the high dimensionality of images while preserving information. Low-level extracted features are utilized for basic qualities automatically derived from an image without requiring shape information or focused on closeness.

The suggested optimized CNN using the PSO algorithm is shown in Fig. 4 as a flowchart.

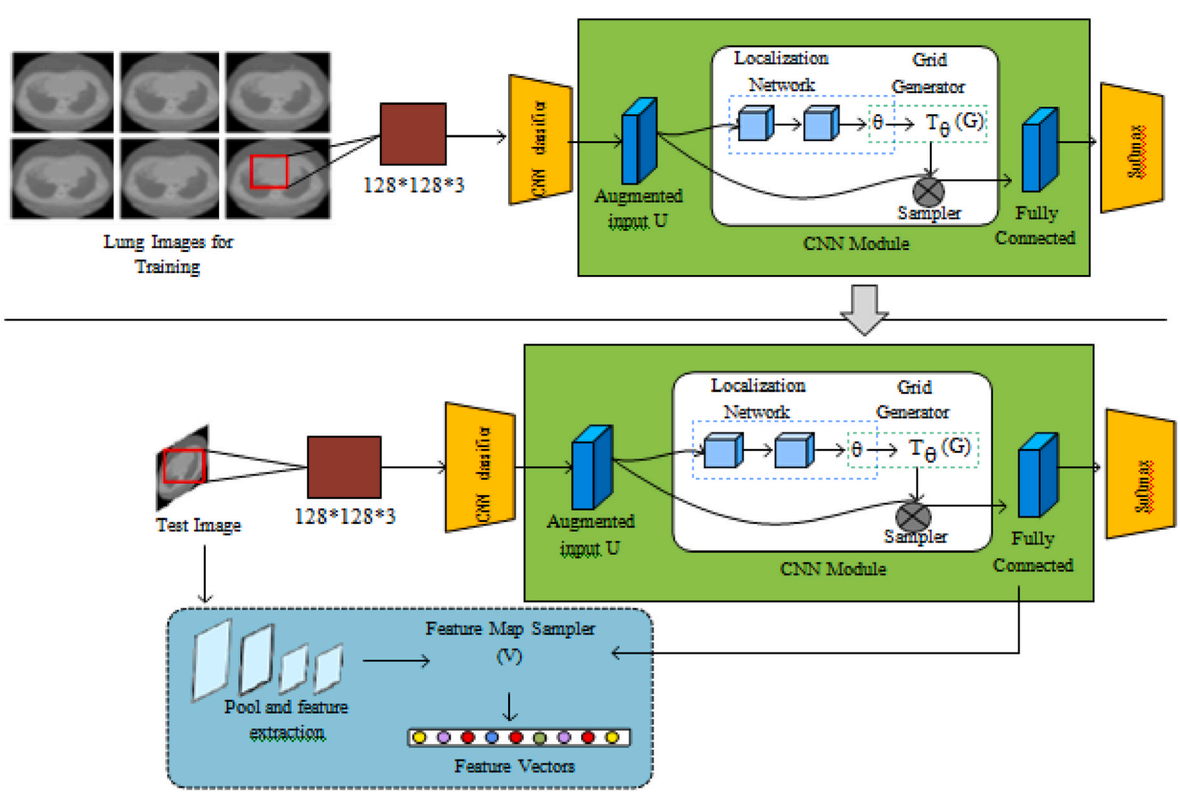

Fig. 3. CNN for categorisation.

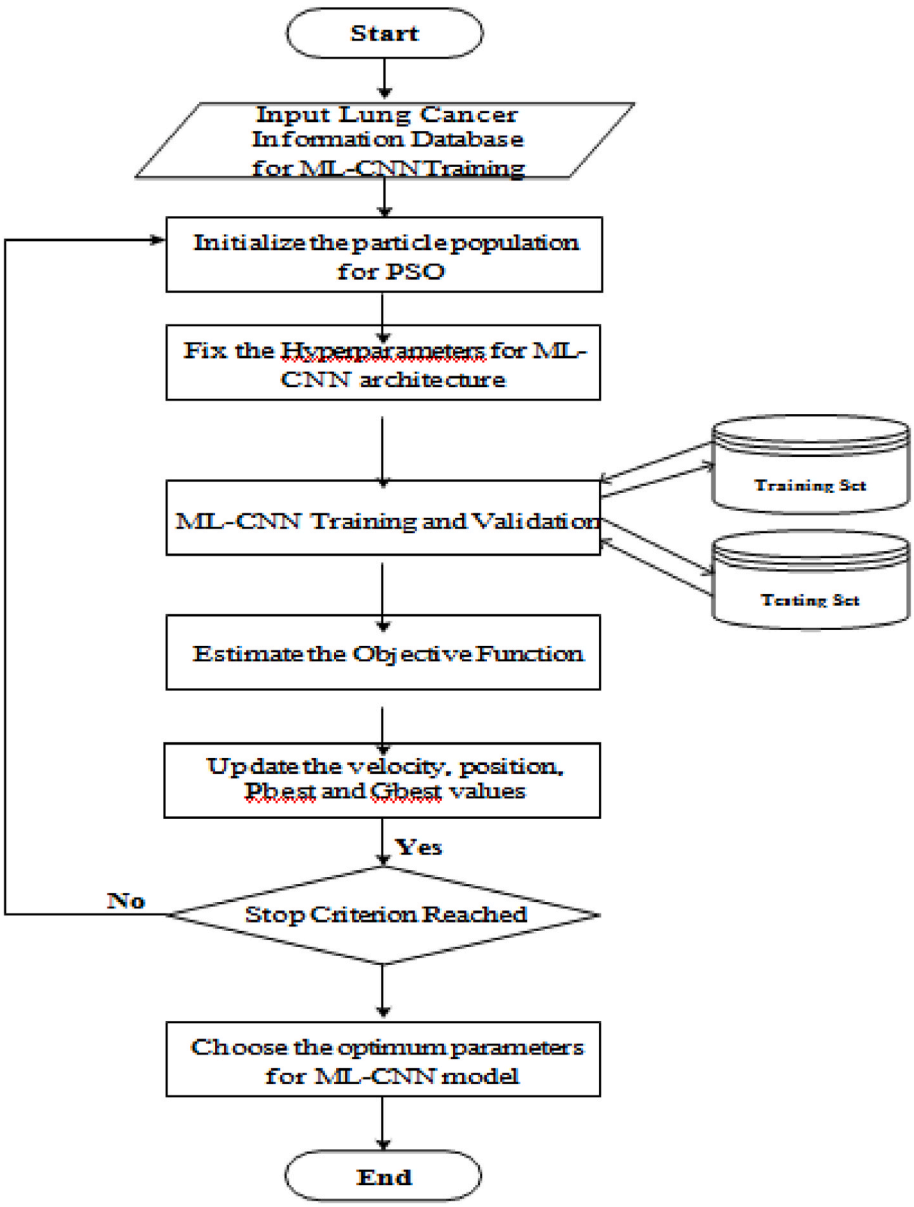

Fig. 4. Flowchart for CNN with Extension of particle swarm Optimization(EPSO).

Following is the computation of the fitness function:

$$fitness_{function} = 1 - \frac{1}{\mathscr{T}} \sum_{j=1}^{\mathscr{T}} \left(x_j - \hat{x}_j\right)^2 \tag{9}$$

The enhanced PSO algorithm updates each particle by computing the neighboring particle's location based on the fitness function, which is modified by the current position.

$$\mathscr{S}_j(n+1) = \left(d_j \times RAND \times \left(g_j^{best} - g_j(n)\right) + d_j \times RAND \times \left(g_k^{best} - g_j(n)\right) + \mathscr{S}_j(n)\right. \tag{10}$$

$$g_j(n+1) = g_j(n) + \mathscr{S}_j(n) \tag{11}$$

The second component in the velocity-updating rule approaches zero if particle $g_j(n)$ is near to the local best g_j^{best}, and the third term approaches zero if particle $g_j(n)$ is close to their global best g_j^{best}. Thus, particles near their global best $g_j best$ or local best $g_j n$ will evolve more readily than those distant from their best ones. Here is how the velocity-updating rule works.

The EPSO method fine-tunes the parameters used in training and testing the whole CNN layer. Performance is optimized by using both local and global search queries. Below is a description of the hybrid CNN with EPSO.

For each iteration, the velocity of the ith particle is represented as $\mathscr{S}_j(n+1)$.

The optimal particle location and coefficient variables are additional variables. The ML-CNN model that has been suggested uses entropy functions in its softmax layer for both illness diagnosis and threshold updates based on the inputs provided. Relative Entropy is used to calculate the similarity between probability distributions, and it is also used to measure an additional entity to determine the threshold values for the classifications. The Square Root of Relative Entropy is used to estimate this additional entity. These steps allow the features to be extracted and appropriately classified. To accurately classify the data, the features in this work are retrieved from the data in a leftward manner. This method uses the following formulas to calculate relative entropy values and the square root of relative entropy. CNN classification pseudocode for machine learning is provided in Algorithm 1 for easy comprehension.

Algorithm 1. ML CNN classification pseudocode

Input: Patterns in perception and images $\mathscr{E}_{ft}$
The size of the whole sequence that has to be categorized is $\mathscr{D}$.
$\mathscr{T}_{j} = 3$//no. of layers
$\mathscr{T}_{e} = 1$//no. of runs
Let $\mathscr{T}_{v}$ = sample number
Let $\mathscr{T}_{f}$ = number of features
Set size testing (n ψd)
20 % is testing and 80 % is training
Make a list of the characteristics by extracting them from the sequence
Let *fft* represent the extracted feature set
Set up CNN settings first
Suppose that batch size is 1
Number of epochs = 1
Let $\mathscr{O}_{av}$ represent the labels for the chosen characteristics
$\mathscr{T}_{d}$ is the number of classes that need to be determined
Load *fft*//load optimized data
For $j = 1$ to $\mathscr{T}_{\mathscr{O}}$
$\mathscr{E}_{fv}$ (feature set) divided into $\mathscr{U}$ (feature subset)
For $i = 1$ to $\mathscr{U}$
To determine backpropagation CNN
For $j = 1$ to size ($n_{\phi d}$)
$\mathscr{T}_{1}.\ \mathscr{E}_{ft} = n_{\phi d}\ (j,)$
End
For $j = 2$: $\mathscr{T}_{\mathscr{O}}$
Layer $= j$
if $\mathscr{T}_{\mathscr{O}}(j) = n_{\phi d}\ (j,)$
Val = $\mathscr{T}_{\mathscr{O}}(j) * n_{\phi d}\ (j,)$
For i = 1:length(Val)
w = 0;
For m = r:length(Val)
Mm = Mm + 1
Val = $\mathscr{T}_{\mathscr{O}}(j-1) * n_{\psi d}$ (m)
Val1 = $\mathscr{T}_{\mathscr{O}}(j) * n_{\psi d}$ (m(;,:,1)
End
End
End
Let $\mathscr{E}_{ft}$ be feature in $\mathscr{E}_{fv}(j, i)$
TCLF estimations with training $\mathscr{E}_{ft}$
Let R_{sort} = sort($\mathscr{U}_{out}$)//rank level
Assume accuracy to be mean($\mathscr{U}_{d\mathscr{O}f}$,1).
$\mathscr{U}_{d\mathscr{O}f} = \sum_{j} (\mathscr{U}_{out} / R_{sort})$
$dtn_j = \Sigma\ (\mathscr{E}_{ft})$ in belonging to samples $\mathscr{T}_{v}$
End
Compute Total count as $\mathscr{D}tn_{\mathscr{U}} = \sum_{j}^{t} \mathscr{D}tn_{j}$
Determine the probability components for every class as
For $j = 1$ to $\mathscr{T}_{d}$
Qcomp(j) = $\mathscr{D}tn_{j} / \mathscr{D}tn_{\mathscr{U}}$
End
End (Ending of firt i for loop)
Output: Classified output

$$\left(\mathscr{E}_{j}, \mathscr{E}_{j+1}\right) = \sum_{m=1}^{t} Q_{j}(M) log \frac{Q_{j}(M)}{Q_{j+1}(M)} \tag{12}$$

$$\mathscr{C}_{SRRE}\left(\mathscr{E}_{j}, \mathscr{E}_{j+1}\right) = \sqrt{\sum_{m=1}^{t} Q_{j}(M) log \frac{Q_{j}(M)}{Q_{j+1}(M)}} \tag{13}$$

5. Experimental results and discussion

5.1. Implementation

In this work, a quick and intelligent approach to detecting lung cancer was developed for use in a medical setting. Using a lung database and a deep learning method, it categorises people with lung issues. Using the ML-CNN technique, the features of the lung were identified. These data serve as a roadmap for the ML-CNN technique's search space, which uses the improved PSO method to find the appropriate class for the inputs once again. Python was the programming language used for the whole investigation. The findings are compiled and arranged in tables and graphs so that they may be compared to other evaluation criteria. Table 1 has the required description. The CNN learns with the help of enhanced PSO algorithms and hyperparameters, which reduce the number of iterations and learning time.

The work is implemented using python and GPU environment in jupyter notebook. For model optimization on low-power IoMT devices, TensorFlow Lite was used. High-performance processing servers and cloud models ARE chosen for storage and processing, to ensure efficient model deployment.

To improve performance and resource utilization for real-time on IoMT devices, the model was optimized for edge devices such as NVIDIA Jetson or Google Edge TPU. This optimization reduces the computational load and reduces energy consumption and ensure the real-time medical decision-making. The model was fine-tuned for low-latency inference, and mini ize the dependence on centralized servers for quick predictions.

The aforementioned parameters are used to avoid overfitting. Both shallow tree and deep tree models are used to compute the hyperparameters. The four-fold validation approach is not a heuristic technique since it may be used with insufficient data.

The numbers mentioned above, referred to as hyperparameters, specify the training needed to create models. The produced model is altered by adjusting the hyperparameters, which are often used to control how the algorithm discovers connections in the data.

To assess the test set's performance, a collection of instances that are not utilized in the training phase or in model tweaking is used. Since this toolkit doesn't leak data into models, it's safe to use to predict how the model will behave in real-world scenarios.

Throughout implementation, different hierarchical models of the enhanced PSO algorithm were modified. These systematic approaches used many performance metrics, all of which were produced by the CNN model. Here is a list of the performance metrics we used in our study.

5.2. Dataset description

➢ The LISS Dataset, a publicly accessible database of common imaging indicators of lung diseases, was accessed on October 19, 2022.

This dataset is known as Longitudinal Internet Studies for the Social Sciences (LISS), CISLTM, and it is available to the public for scholarly and research purposes. It includes roughly nine lung nodule signals taken at the Chinese Academy of Medical Sciences Cancer Institute and Hospital, 511 2D CISLs for 252 patients, and 166 3D photos for 19 patients. The Toshiba Aquilion 64 Slice CT scanner and the GELight Speed VCT-64, located in Holt, Michigan, USA, produced these pictures. DICOM 3.0 is the image format. The nine lung nodule sign pictures in the LISS database encompass 2D occurrences, whereas ground-glass opacity (GGO) is the sole sign covering 3D examples.

Each CT picture has a matching label in LISS, and the size of each image is expressed in pixels. This database's abundance of lung photos with various nodule signals is the primary reason we gave it any

Table 1
Hyperparameters of CNN and enhanced PSO.

Methods Used	Parameters	Description
CNN	Number of Epochs	5
	Non-Linear Activation Function	ReLU
	Activation Function	Softmax
	Learning Function	Adam Optimizer
EPSO	Number of Particles	10
	Iterations	10
	Inertial Weight (W)	0.85
	Social Constant (W2)	2
	Cognitive Constant (W1)	2

Table 2
Dataset description.

CT Imaging Scans	Annotated ROIs	
	19–3D	166–3D
Lobulation	21	41
Calcification	20	47
Cavity and Vacuoles	75	147
Speculation	18	29
Pleural Dragging	26	80
Air Bronchogram	22	23
Bronchial Mucus Plugs	19	81
Sum	271	677
Obstructive Pneumonia	16	18

thought. In every class, the lung imaging slice size ranges from 0.418 to 1 mm, with an average slice value of 0.664 mm. Table 2 shows the description of the LISS database, which is divided into two groups: annotated ROIs and CT imaging scans.

The LISS database stores the CT imaging scans as plain text, and each annotated ROI CT picture is kept as a separate file for each nodule sign. The following lists each nodule sign's description.

- GGO: This is a sign indicating vascular and bronchial borders with fuzzy maximized attenuation. Both lung adenocarcinoma and bronchioloalveolar carcinoma are suggested by it.
- Lobulation: A malignant lesion may indicate the growth of connective tissue septae, which include fibroblasts identified as originating from the perithymic mesenchyme.
- Calcification: This indicates that insoluble salts, such as calcium and magnesium, have deposited. Its features, including shape and location, are important in determining whether a lung nodule is cancerous or benign. The centre areas of lesions, spotted lesions, and uneven appearance indicate malignancy, whereas popcorn and thick calcifications suggest that the lung imaging is benign. It is calculated using high-density pixel lung nodule regions, and CT scan ranges are more than 100 HU (Hounsfield Units).
- Cavity and Vacuoles: These indicate hollow spaces symbolized by tissues. Cavities include the vacuole. The hollow is associated with tumours larger than 3 mm, and it is indicative of bronchioloalveolar carcinoma and adenocarcinoma.
- Hypothesis: Stellate deformation in tissue lesions is the source of this symptom. This is one of the typical lung nodule indications associated with a desmoplastic response brought on by the entry of the malignant tumour. According to this finding, lung parenchyma extends from the fibrotic thread. It indicates a cancerous tumour.
- Pleural indentation indicates a tumor-affected region that has been identified in the tissues. The indication is associated with peripheral adenocarcinomas of fibrotic and anthracitic foci in the central or subpleural region.
- Another name for them is focal opacities, or bronchial mucus plugs (BMPs). Their densities range from less than 100 HU to more than 100 HU for liquefied states. Their cause is allergic bronchopulmonary aspergillosis, and they are the result of mucus-transformed intrabronchial air.
- An air branchogram indicates the development of low-attenuation bronchi on top of a high-attenuation airless lung. The causes are as follows: (1) proximal airway patency; (2) alveolar air removal, which results in either absorption (atelectasis) or replacement (pneumonia); or (3) the coexistence of both symptoms. Rarely, lymphoma, or significant interstitial expansion, is the cause of air displacement.
- A rectangular mark that indicates a tiny lung nodule volume caused by the distal collapse in obstructive pneumonia. Proximal bronchial obstruction is mostly to blame for this. Alongside squamous cell carcinoma and adenocarcinoma, it is combined. The cuneate or flabellate region with increased density is shown visually by this. The Ground-glass opacity(GGO), Cavity and Vacuoles, Lobulation, Bronchial Mucus Plugs, and Pleural Indentation are considered to be the malignant lung nodule lesions, according to radiologists' assessments of lung nodule indicators. Benign or malignant lesions are distinguished by air biopsy, obstructive pneumonia, and calcification criteria.

➢ LIDC-IDRI Dataset

Thoracic CT scan pictures (1018 CT scan images) from 1010 patients make up the LIDC-IDRI dataset, the largest publicly accessible collection for academics worldwide Fig. 5. These images demonstrate the existence of nodule markings, or outline-like features, together with lung tumours. For every patient, there are nodule annotations accessible. Nevertheless, the diagnostic data is provided for 157 individuals in the form of ratings for nodules, with 0 denoting an unknown class, 1 the benign class, 2 the main malignant class, and 3 the metastatic (malignant) class.

Every picture receives a rating based on a biopsy, surgical resection, progression, and radiological image revision. There are two groups under-diagnosis: (i) patient level and (ii) nodule level. Images from 1000 patients were gathered over an extended period using various CT scanners to create this dataset for radiologists. Table 3 displays the diameter size distribution of lung nodules in the Lung Image Database Consortium (LIDC)- Infectious Disease Research Institute (IDRI) database. The various slices are accompanied by several lung nodules. Annotated data is included with every lung nodule slice, and the existence of each nodule is determined by a 3 mm size.

Malignancy may be determined using diagnostic data in the LIDC database. The ratings were selected based on diagnostic data; the ground truth was prepared for training in the triplet Content-Based Medical Information Request (CBMIR) system and assessed by contrasting the outcomes with the ratings provided by radiologists in the database. Annotations for the nodules in the yellow box, which range in size from 3 mm to 30 mm, are available from this database.

5.3. Performance measures

Equation (14) displays the accuracy rate as the number of correct sickness estimations is divided by the total number of diagnoses. Equation (15) provides the prediction result's ability to accurately identify individuals who do not exhibit any lung ailment risk indicators. It stands for precision. Fig. 8 provides an estimate of sensitivity, which is the ability of a decision result to accurately identify individuals with the disease.

The precision for a category is equal to the number of actual positives (i.e., risk controls and indicators for individuals in the true-positive group) divided by the total number of individuals identified by the classification model (i.e., the total number classified as positive outcomes, including components mistakenly labeled as belonging to the positive class).

The F-Score, the harmonized average mean of the specificity and sensitivity ratings. The total time lag between learning and assessing the computational model is known as the processing time delay. Equation (15) illustrates it. In the following sections, the lung cancer diagnostic model's performance is examined and contrasted with other approaches.

$$ACC = \frac{TP + TN}{TP + TN + FP + FN} \times 100\%$$

$$Sensitivity = \frac{TP}{TP + TN} \times 100\%$$

$$Specificity = \frac{TN}{TN + FP} \times 100\%$$

$$Precision = \frac{TP}{TP + FP} \times 100\%$$

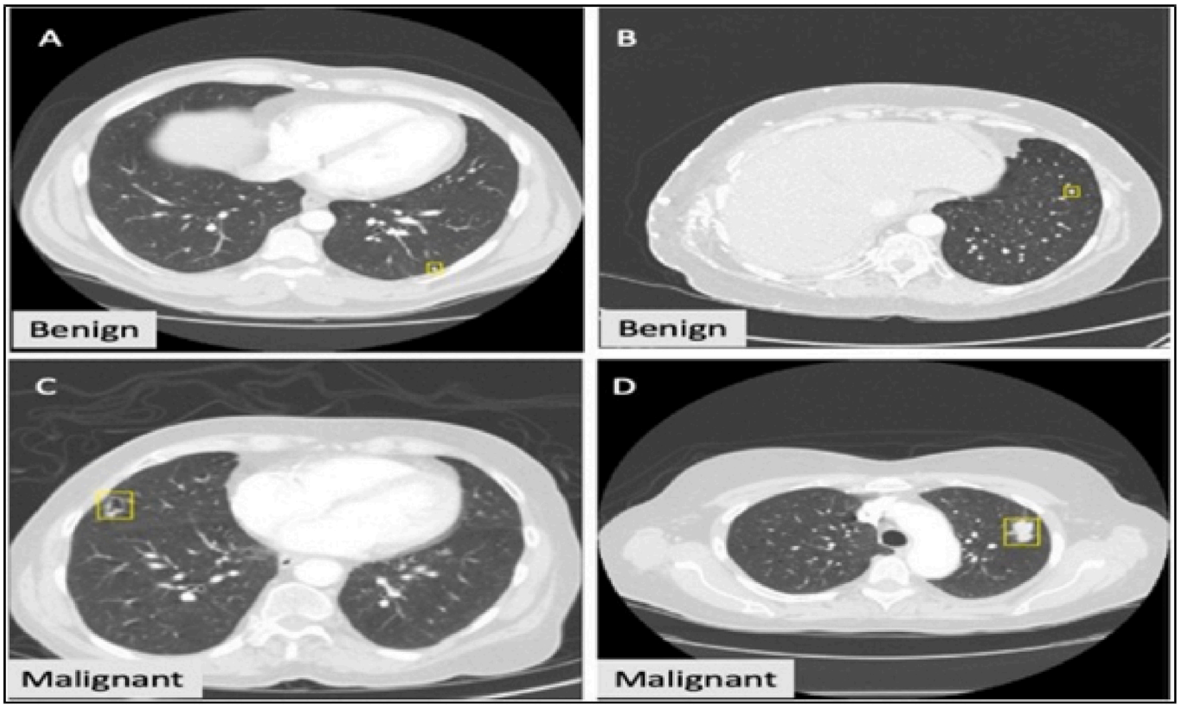

Fig. 5. Lung classification results.

Table 3
LIDC-IDRI database description.

Nodule Description	Number of Nodules
No. of nodules or lesions marked by at least one radiologist	7371
No. of <3 mm nodules marked by at least one radiologist	2669
No. of <3 mm nodules marked by all four radiologists	928

$$F-Score = \frac{2*precision*sensitivity}{precision + sensitivity} \times 100\%$$

Where TP = true positive, TN = true negative, FP = false positive, FN = false negative.

Based on the number of occurrences, the model's performance is shown in Figs. 6–10 in terms of accuracy, sensitivity, specificity, precision, and execution time. The suggested ML-CNN technique performs best for lung cancer diagnosis, as seen by the findings displayed in the figures. The suggested ML-CNN technique has achieved maximum performance via efficient data collecting, image preprocessing, extracted features, chosen features, and classification by parameter adjustment. The performance is enhanced by the resolution of issues related to low-quality photos, inadequate data, and features. Moreover, the suggested approach computes the filtering accuracy, and the current approaches bolster the classification accuracy when the emphasis is on image-based lung cancer detection.

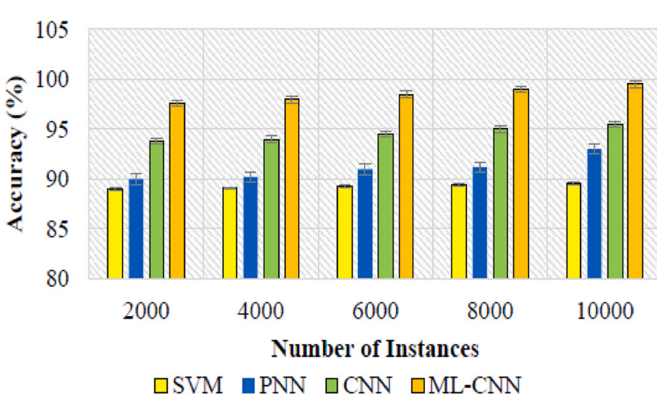

Fig. 6. Accuracy vs. number of instances.

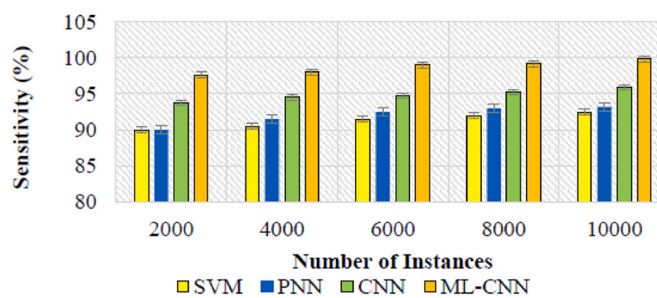

Fig. 7. Sensitivity vs. number of instances.

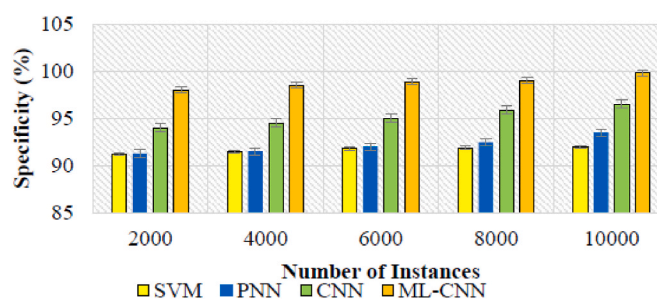

Fig. 8. Specificity vs. number of instances.

After selecting visual and semantic characteristics, they denoise to eliminate potential noise. Filtering accuracy was examined to assess the effectiveness of the approach used in this work. This filtering accuracy statistic defines the range of filtering or whether the noise-containing frames are eliminated. The inverse of the mean square error, provided as, is used to determine the filtering accuracy.

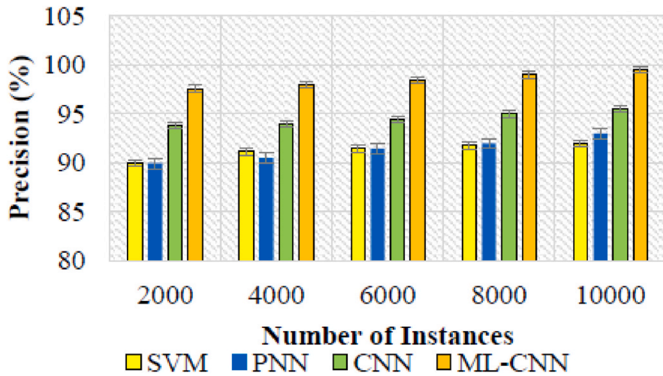

Fig. 9. Precision vs. number of instances.

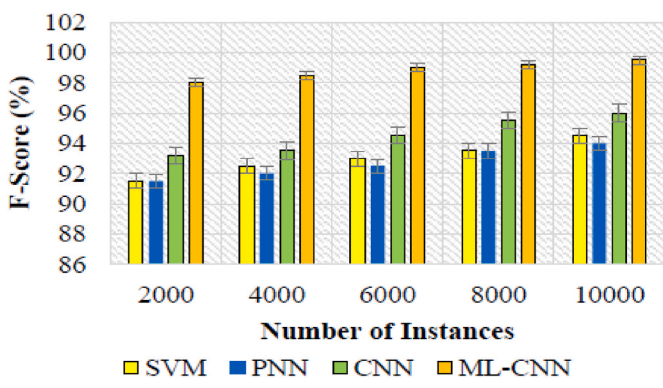

Fig. 10. F-score vs. number of instances.

$$Filter\ accuarcy = \left(\frac{1}{MSE}\right)*100\% \tag{14}$$

$$MSE = \frac{1}{t}\sum_{j=1}^{t}\left(\widehat{x_j} - x_j\right)^2 \tag{15}$$

Equation (15) shows that the mean is $\frac{1}{t}\sum_{j=1}^{t}\left(\widehat{x_j} - x_j\right)^{2,}$ and the square of errors is $\left(\widehat{x_j} - x_j\right)^2$. The specified formulation was used to determine the filtering accuracy, and the results are satisfactory. This study effort compared the prior rapid bilateral filter used to remove noise from pictures with the suggested Bayesian threshold approach. Figs. 11 and 12 provide the comparative analysis of execution time and computational demand with the models of SVM, PNN, CNN and ML-CNN. When compared with the other models the suggested model achieves notable efficacy in terms of execution time and computational load.

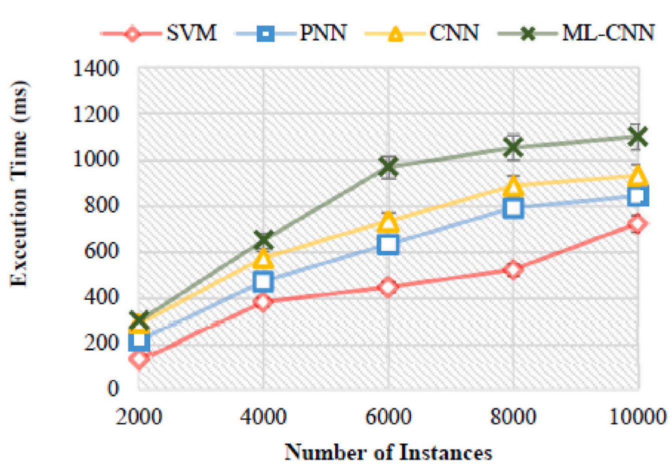

Fig. 11. Execution time vs. number of instances.

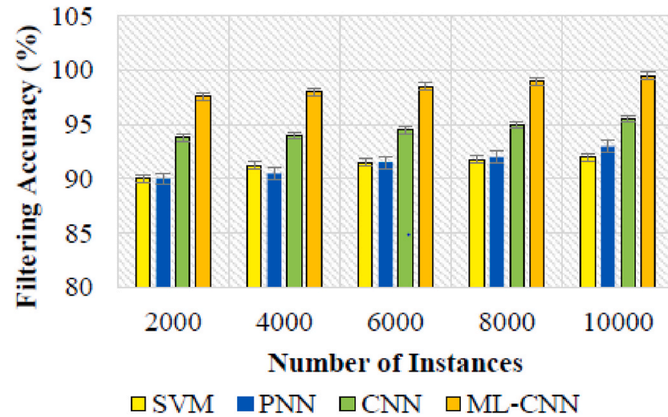

Fig. 12. Filtering accuracy vs. number of instances.

On the other hand, a quick bilateral filter concentrates on eliminating noise that is only present at the diagnosis. This is the primary cause of the quick bilateral filters' decreased filtering accuracy. The comparison graph demonstrates a steady rise in filtering accuracy over time. The classification accuracy likewise increases because the quality of the pictures improves with an increase in this parameter. Next, a comparison based on optimization was conducted between the suggested and earlier methods. This paper used the Enhanced PSO method to adjust hyperparameters and contrasted them with classical approaches. Table 4 shows the numerical results of existing and proposed. According to Table 4, we investigate the tradeoff based on precision and sensitivity at different attack levels. In EPSO, 2000 attacks the precision is 98.23 % and sensitivity is 98.25 %. This highlights that the model effectively reduces false positives and accurately identifies the true positives with low attack levels. However, in the 10000 attacks range, the precision increases by 98.89 % but shows a slight decrease to 98.45. This highlights that the model becomes more focused on reducing false positives by missing some true positives. This is possible in high-attack range scenarios.

We examined the recommended method utilising a range of PSO-selected characteristics to assess its performance metrics. At the

Table 4
Comparison of numerical results for proposed and existing methods.

Algorithm	Attacks	Accuracy (%)	Precision (%)	Sensitivity (%)	Specificity (%)	F1-Measure (%)
GA	2000	84.52	86.75	85.45	86.75	85.7
	4000	86.54	87.45	86.12	87.45	85.9
	6000	87.45	88.15	86.75	88.78	85.6
	8000	88.02	88.16	86.78	88.95	85.9
	10,000	88.15	88.19	86.79	88.23	86
ACO	2000	88.45	88.78	88.91	88.96	89
	4000	88.6	88.75	88.90	88.97	89.15
	6000	88.69	88.89	88.92	88.98	89.45
	8000	88.72	88.90	88.94	88.98	89.55
	10,000	89.75	88.91	88.95	88.99	89.6
BCO	2000	90.1	91.23	91.25	91.44	91.63
	4000	90.25	91.45	91.35	91.56	91.65
	6000	90.26	91.75	91.39	91.58	91.67
	8000	90.32	91.88	91.40	91.60	91.69
	10,000	90.45	91.89	91.45	91.62	91.85
EPSO	2000	98.1	98.23	98.25	98.44	98.63
	4000	98.25	98.45	98.35	98.56	98.65
	6000	98.26	98.75	98.39	98.58	98.67
	8000	98.32	98.88	98.40	98.60	98.69
	10,000	98.45	98.89	98.45	98.62	98.85

maximum degree of accuracy, F1 = 0.6, F2 = 0.5, and h = 1.0 are found. The test results for the different parameters are shown in Table 5. The ideal empirical combination of particle and iteration numbers was determined after early testing. The ultimate performance values in Table 6 were achieved after 2500 particles and 29 iterations. The performance for various features is presented in Table 7.

Tables 5–7 include information on EPSO data, EPSO iterations, and a feature that helps the model predict outcomes more accurately.

Understanding the AUC-ROC curve is essential for evaluating a model's performance when identifying an instance belonging to either positive or negative classes. The area underneath the curve (AUC) acts as a coefficient of determination for the model's classification capacity; thus, the closer it is to 1.0, the more accurate the classification, whereas 0.5 suggests the model is just as effective as a monkey tossing a coin.

The curve in Fig. 13 shows the relationship between sensitivity and the false positive rate, which allows users to see the effect of various cut-off points on the model's performance. This is also important when a diagnosis in the medical field has to be made, as a trade-off between sensitivity and specificity is required (see Fig. 14).

Convolutional Neural Networks (CNN) fusion with advanced Particle Swarm Optimization (PSO) aims to increase classification accuracy. With better tuning of hyperparameters, the model can better differentiate between benign and malignant tumours, achieving better diagnostic results. The ML-CNN with PSO aims not only to improve the sufficiency of the testing process but also to minimise errors and defaults on which the decision is based, which is essential in healthcare settings. Table 8 compares the proposed work, and Table 9 shows the model's 4-fold cross-validation.

6. Conclusions

One of the advantages of IoT-based healthcare facilities is virtual access to health imaging, particularly computed tomography for lung cancer. it is now more straightforward to use age data gathered by several servers to look into sickness patterns. Consequently, cancer may be diagnosed by using this data for CNN training. In this work, we built a novel classifier based on a comprehensive, fully convolutional neural network. Biological images may be identified and categorized using ML-CNN, a wide-sense classifier. However, in this study, pulmonary nodules in CT scan pictures are identified and categorized using ML-CNN. Two categories are used to train the proposed ML-CNN classifier: nodule (diseased—malignant or normal) and non-nodule (non-diseased—malignant or benign) (standard). Before being sent to the ML-CNN with PSO for feature extraction and classification, the sensor data is first preprocessed using the normalization technique. Subsequently, the lung images undergo preprocessing using a Bayesian threshold based on the Taylor series for noise reduction. The intensity values are subsequently normalized using Z-score normalization. Next, the PSO technique is used to adjust the hyperparameters, improving performance, and the lung-image-based information, including colour, shape, and intensity, is retrieved from the picture.

In that order, the accuracy, precision, sensitivity, specificity, and F-measure values of ML-CNN with EPSO are 98.45, 98.89, 98.45, 98.62, and 98.85. Comparing the hybrid technique to other methods yields higher convergence outcomes with higher accuracy. The learning process in deep learning is regulated by parameters called hyperparameters.

Table 5
Algorithm parameters for EPSO using empirical data.

F1	F2	h	Accuracy
0.8	0.6	1.0	98.45
0.8	0.6	0.9	97.73
0.8	0.6	1.0	98.12
0.7	0.6	1.0	98.09
0.6	0.5	1.0	99.46

Table 6
EPSO technique outcomes with increasing numbers of iterations and a constant number of particles.

	Iterations	Accuracy	Precision	F-Measure
2500	25	97.90	97.89	97.12
2500	26	98.06	97.03	97.56
2500	27	98.45	96.43	96.49
2500	28	98.23	97.63	98.62
2500	29	99.56	99.54	99.32
2500	30	97.96	97.87	97.51

Table 7
EPSO algorithm observations with various feature sizes.

Features	Accuracy	Precision	F-Measure
10	99.45	99.03	99.89
12	98.09	97.46	97.43
15	98.83	98.03	98.69
18	98.23	98.67	97.52
20	97.12	97.23	98.86

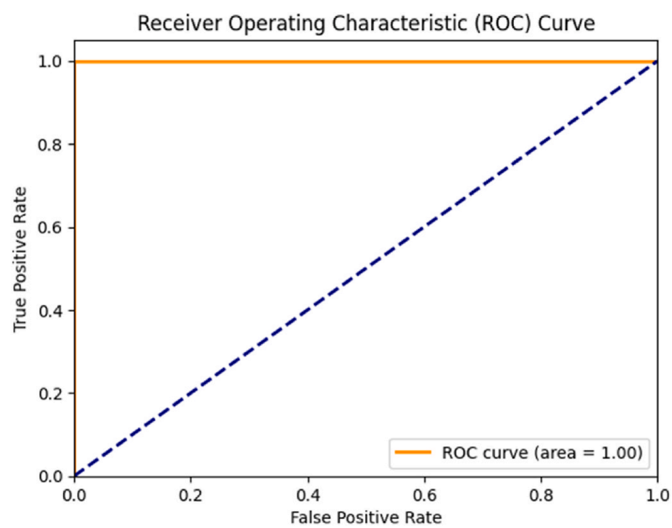

Fig. 13. AUC-ROC model for proposed work.

The hyperparameters may be adjusted to gain more excellent performance while searching for hidden features of the CNN, such as colour, shape, and intensity. Model hyperparameters are manually specified to assist in estimating model parameters. Because they need human fine-tuning in machine learning, model hyperparameters are often referred to as parameters.

CNN is assisted in feature extraction and classification by EPSO, which raises the accuracy, precision, sensitivity, specificity, and F-measure for both EPSO and hyperparameters.

Future research will focus on expanding the proposed framework to cardiovascular diseases, diabetic retinopathy, and neurological disorders, possibly by applying it to various medical imaging datasets. To classify other CT picture types, such as melanoma, mammography, and heart imaging, we want to use more lung datasets in future studies and apply hypotheses via fine-tuning and transfer learning. The ongoing research will also assess the model's generalisation for other medical imaging. Integrating multi-modal data can enhance the precision of the lung cancer detection system. Combining imaging data with genetic information (e.g., mutations, biomarkers) could enable personalised cancer predictions and improve detection accuracy. However, for effective implementation in actual clinical settings, issues regarding data overload, device compatibility, and the security and privacy of IoT-enabled devices must be resolved.

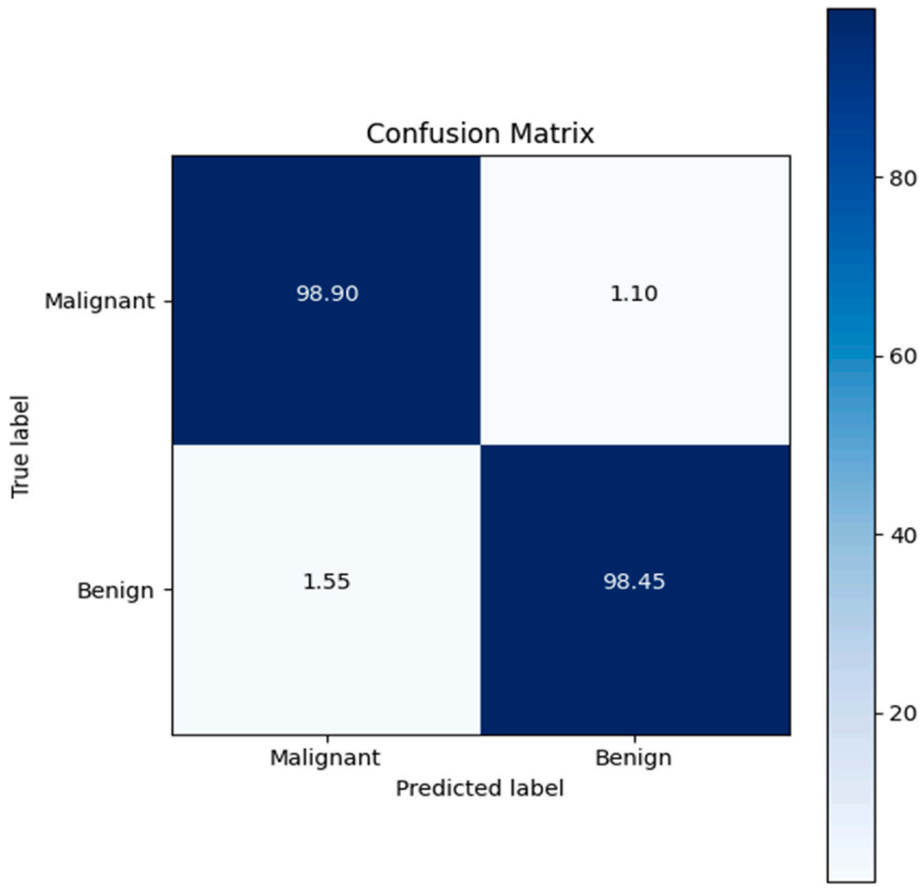

Fig. 14. Confusuion matric.

Table 8
Comparison of existing and proposed work.

Model	Dataset	Accuracy%
Resnet-152,Densenet-169,efficientnet-b7 (Gautam et al., 2024)	LIDC-IDRI	97.23
Multi-Layer Perceptron (MLP) and convolution neural network (DenseNet201). (Shanshool et al., 2023)	LIDC-IDRI	99.3
NoduleDiag (Alshayeji and Abed, 2023)	LIDC-IDRI	99.6
Proposed model	LIDC-IDRI	Till 98.9–99.8

Table 9
Cross validation of the model.

Fold	Accuracy (%)	Precision (%)	Sensitivity (%)	Specificity (%)	F1-Score (%)
Fold 1	98.9	98.89	98.45	98.62	98.85
Fold 2	99.0	98.90	98.50	98.63	98.86
Fold 3	99.2	98.92	98.55	98.64	98.87
Fold 4	99.8	98.91	98.48	98.60	98.86

CRediT authorship contribution statement

Xin Hou: Writing – review & editing, Visualization, Validation, Supervision. **Nisreen Innab:** Writing – review & editing, Visualization, Validation. **Saad Alahmari:** Writing – review & editing, Validation, Software. **Meshal Shutaywi:** Writing – review & editing, Supervision, Resources, Project administration. **Sara A. Althubiti:** Writing – review & editing, Supervision, Resources, Funding acquisition. **Ali Ahmadian:** Writing – review & editing, Visualization, Validation, Supervision.

Declaration of competing interest

The authors declare that they have no known competing financial interests or personal relationships that could have appeared to influence the work reported in this paper.

Acknowledgment

This research study is partially supported by fund titled "the mechanism by which protein argininedeiminase moduates macrophadephenotype to promote the transformationfrom COPD to lung cancer", Henan Province Medical Science and Technology Joint Research Program (LHGJ20240384). The authors extend their appreciation to the Deanship of Scientific Research at Northern Border University, Arar, KSA, for funding this research work through the project number "NBU-FPEJ-2025-451-06". Also, this research study is supported by "Researchers Supporting Project number (MHIRSP2024013)", Almaarefa University , Riyadh, Saudi Arabia.

Data availability

Data will be made available on request.

References

Abd El-Aziz, R.M., Alanazi, R., Shahin, O.R., Elhadad, A., Abozeid, A., Taloba, A.I., Alshalabi, R., 2022. An effective data science technique for IoT-Assisted healthcare monitoring system with a rapid adoption of cloud computing. Comput. Intell. Neurosci. 2022.

Alshayeji, M.H., Abed, S., 2023. Lung cancer classification and identification framework with automatic nodule segmentation screening using machine learning. Appl. Intell. 53, 19724–19741. https://doi.org/10.1007/s10489-023-04552-1.

Alsinglawi, B., Alshari, O., Alorjani, M., Mubin, O., Alnajjar, F., Novoa, M., Darwish, O., 2022. An explainable machine learning framework for lung cancer hospital length of stay prediction. Sci. Rep. 12 (1), 607.

Arumugam, S.R., Bhushan, B., Arya, M., Manoj, O., Basha, S.M., 2022. Lung cancer detection using modified fuzzy C-means clustering and adaptive neuro-fuzzy network. In: Applications of Artificial Intelligence and Machine Learning: Select Proceedings of ICAAAIML 2021. Springer Nature Singapore, Singapore, pp. 733–742.

Bharathy, S., Pavithra, R., 2022. Lung cancer detection using machine learning. In: 2022 International Conference on Applied Artificial Intelligence and Computing (ICAAIC). IEEE, pp. 539–543.

Civit-Masot, J., Bañuls-Beaterio, A., Domínguez-Morales, M., Rivas-Pérez, M., Muñoz-Saavedra, L., Corral, J.M.R., 2022. Non-small cell lung cancer diagnosis aid with histopathological images using Explainable Deep Learning techniques. Comput. Methods Progr. Biomed. 226, 107108.

Dodia, S., Annappa, B., Mahesh, P.A., 2022. Recent advancements in deep learning based lung cancer detection: a systematic review. Eng. Appl. Artif. Intell. 116, 105490.

Duan, Xingguang, Xie, Dongsheng, Zhang, Runtian, Li, Xiaotian, Sun, Jiali, Qian, Chao, Song, Xinya, Li, Changsheng, 2023. A novel robotic bronchoscope system for navigation and biopsy of pulmonary lesions. Cyborg Bionic Syst 4, 0013.

Feng, X., Ma, Z., Yu, C., Xin, R., 2024. MRNDR: multihead attention-based recommendation network for drug repurposing. J. Chem. Inf. Model. 64 (7), 2654–2669.

Gautam, N., Basu, A., Sarkar, R., 2024. Lung cancer detection from thoracic CT scans using an ensemble of deep learning models. Neural Comput & Applic 36, 2459–2477. https://doi.org/10.1007/s00521-023-09130-7.

Hasenleithner, S.O., Speicher, M.R., 2022. A clinician's handbook for using ctDNA throughout the patient journey. Mol. Cancer 21 (1), 81.

Hosseini, S.H., Monsefi, R., Shadroo, S., 2024. Deep learning applications for lung cancer diagnosis: a systematic review. Multimed. Tool. Appl. 83 (5), 14305–14335.

Hu, F., Yang, H., Qiu, L., Wei, S., Hu, H., et al., 2025. Zhou, H, Spatial structure and organization of the medical device industry urban network in China: evidence from Specialized, Refined, Distinctive, and Innovative firms. Front. Public Health 13.

Huang, H., Wu, N., Liang, Y., Peng, X., Shu, J., 2022. SLNL: a novel method for gene selection and phenotype classification. Int. J. Intell. Syst. 37 (9), 6283–6304.

Jiang, Y., Chen, R., Xu, S., Ding, Y., Zhang, M., Bao, M., et al., 2024. Endocrine and metabolic factors and the risk of idiopathic pulmonary fibrosis: a mendelian randomization study. Front. Endocrinol. 14.

Kapatia, G., Saikia, A., Mohapatra, D.S., Gupta, P., Rohilla, M., Gupta, N., Srinivasan, R., Rajwanshi, A., Dey, P., 2023. The cytological diagnosis of Pneumocystis jiroveci pneumonia in bronchoalveolar lavage. CytoJournal 20.

Kobylińska, K., Orłowski, T., Adamek, M., Biecek, P., 2022. Explainable machine learning for lung cancer screening models. Applied Sciences 12 (4), 1926.

Li, H., Jiang, Y., Wang, Y., Lv, H., Xie, H., Yang, G., et al., 2018. The effects of warfarin on the pharmacokinetics of senkyunolide I in a rat model of biliary drainage after administration of chuanxiong. Front. Pharmacol. 9.

Li, H., Zhou, Y., Liao, L., Tan, H., Li, Y., Li, Z., et al., 2023. He, B, Pharmacokinetics effects of chuanxiong rhizoma on warfarin in pseudo-germ-free rats. Front. Pharmacol. 13, 1022567.

Li, C., Wang, H., Wen, Y., Yin, R., Zeng, X., et al., 2024a. GenoM7GNet: an efficient N7-methylguanosine site prediction approach based on a nucleotide language model. IEEE ACM Trans. Comput. Biol. Bioinf 1–11.

Li, Q., You, T., Chen, J., Zhang, Y., Du, C., 2024b. LI-EMRSQL: linking information enhanced Text2SQL parsing on complex electronic medical records. IEEE Trans. Reliab. 73 (2), 1280–1290.

Lin, L.P., Tan, M.T.T., 2023. Biosensors for the detection of lung cancer biomarkers: a review on biomarkers, transducing techniques and recent graphene-based implementations. Biosens. Bioelectron., 115492

Lin, X., Liao, Y., Chen, X., Long, D., Yu, T., et al., 2016. Regulation of oncoprotein 18/stathmin signaling by ERK concerns the resistance to taxol in nonsmall cell lung cancer cells. Cancer Biother. Rad. 31 (2), 37–43.

Luan, S., Yu, X., Lei, S., Ma, C., Wang, X., Xue, X., et al., 2023. Deep learning for fast super-resolution ultrasound microvessel imaging. Phys. Med. Biol. 68 (24).

Lydia, M.D., Prakash, M., 2023. An automatic lung nodule detection and classification using an optimized convolutional neural network and enhanced k-means clustering. J. Ambient Intell. Hum. Comput. 14 (12), 16973–16984.

Malik, H., Anees, T., Din, M., Naeem, A., 2023. CDC_Net: multi-classification convolutional neural network model for detection of COVID-19, pneumothorax, pneumonia, lung Cancer, and tuberculosis using chest X-rays. Multimed. Tool. Appl. 82 (9), 13855–13880.

Manickam, M., Siva, R., Prabakeran, S., Geetha, K., Indumathi, V., Sethukarasi, T., 2022. Pulmonary disease diagnosis using African vulture optimized weighted support vector machine approach. Int. J. Imag. Syst. Technol. 32 (3), 843–856.

Pandian, R., Vedanarayanan, V., Kumar, D.R., Rajakumar, R., 2022. Detection and classification of lung cancer using CNN and Google net. Measurement: Sensors 24, 100588.

Patil, J.K., Dhole, S.A., Mandlik, V.S., Patil, V.D., 2023. Detection of Lung Cancer from CT Scan Images Using GLCM Features.

Rajasekar, V., Vaishnnave, M.P., Premkumar, S., Sarveshwaran, V., Rangaraaj, V., 2023. Lung cancer disease prediction with CT scan and histopathological images feature analysis using deep learning techniques. Results in Engineering 18, 101111.

Rikta, S.T., Uddin, K.M.M., Biswas, N., Mostafiz, R., Sharmin, F., Dey, S.K., 2023. XML-GBM lung: an explainable machine learning-based application for the diagnosis of lung cancer. J. Pathol. Inf. 14, 100307.

Shanshool, A.M., Bouchakwa, M., Amor, I.A.B., 2023. Improved accuracy of pulmonary nodule classification on LIDC-IDRI dataset using deep learning. Procedia Comput. Sci. 225, 394–403.

Sivakumar, V., Yogesh, C.K., Vatchala, S., Kaliraj, S., 2024. An efficient lung image classification and detection using spiral-optimized Gabor filter with convolutional neural network. Int. J. Imag. Syst. Technol. 34 (1), e23013.

Su, Y., Tian, X., Gao, R., Guo, W., Chen, C., Chen, C., et al., 2022. Lv, X, Colon cancer diagnosis and staging classification based on machine learning and bioinformatics analysis. Comput. Biol. Med. 145.

Thanoon, M.A., Zulkifley, M.A., Mohd Zainuri, M.A.A., Abdani, S.R., 2023. A review of deep learning techniques for lung cancer screening and diagnosis based on CT images. Diagnostics 13 (16), 2617.

Trivedi, S., Patel, N., Faruqui, N., 2022. A novel lightweight lung cancer classifier through hybridization of DNN and comparative feature optimizer. In: International Conference on Hybrid Intelligent Systems. Springer Nature Switzerland, Cham, pp. 188–197.

Vishwa Kiran, S., Kaur, I., Thangaraj, K., Saveetha, V., Kingsy Grace, R., Arulkumar, N., 2023. Machine learning with data science-enabled lung cancer diagnosis and classification using computed tomography images. Int. J. Image Graph. 23 (3), 2240002.

Wang, B., Chen, W., Qian, J., Feng, S., Chen, Q., et al., 2025. Single-shot super-resolved fringe projection profilometry (SSSR-FPP): 100,000 frames-per-second 3D imaging with deep learning. Light Sci. Appl. 14 (1), 70.

Wani, N.A., Kumar, R., Bedi, J., 2024. DeepXplainer: an interpretable deep learning based approach for lung cancer detection using explainable artificial intelligence. Comput. Methods Progr. Biomed. 243, 107879.

Xu, Y., Wang, Y., Razmjooy, N., 2022. Lung cancer diagnosis in CT images based on Alexnet optimized by modified Bowerbird optimization algorithm. Biomed. Signal Process Control 77, 103791.

Yan, R., Shen, Y., Zhang, X., Xu, P., Wang, J., Li, J., et al., 2023. Histopathological bladder cancer gene mutation prediction with hierarchical deep multiple-instance learning. Med. Image Anal. 87, 102824.

Yu, X., Luan, S., Lei, S., Huang, J., Liu, Z., Xue, X., et al., 2023. Deep learning for fast denoising filtering in ultrasound localization microscopy. Phys. Med. Biol. 68 (20).

Zaidi, T., Sushma, B.S., 2023. Applications of machine learning in healthcare with a case study of lung cancer diagnosis through deep learning approach. In: AI and Blockchain in Healthcare. Springer Nature Singapore, Singapore, pp. 95–104.